Remote Sensing in Ecology and Conservation

Zoological Society of London

ORIGINAL RESEARCH OPEN ACCESS

Mapping Middens: Multimodal Imagery Illuminates Rhino Space Use in Savanna Landscapes

Catherine A. Ressijac[1] | Lucia Gordon[2] | Andrew B. Davies[1]

[1]Department of Organismic and Evolutionary Biology, Harvard University, Cambridge, Massachusetts, USA | [2]John A. Paulson School of Engineering and Applied Sciences, Harvard University, Allston, Massachusetts, USA

Correspondence: Catherine A. Ressijac (catherine_ressijac@g.harvard.edu)

Received: 30 June 2026 | **Revised:** 1 October 2026 | **Accepted:** 21 October 2026

Editor: Anna Cord | **Associate Editor:** Gaia Vaglio Laurin

Keywords: *Ceratotherium simum* | *Diceros bicornis* | dung pile | feature detection | latrine | thermal imagery | UAV

ABSTRACT

Ecosystem engineering by many animal species creates distinct features across landscapes that shape biodiversity and ecosystem structure and serve as key signatures of animal space use. Remote sensing has been used to map the spatial distributions of such features across landscapes, enhancing our ability to characterize the biotic factors that create resource heterogeneity. However, some animal-engineered features are challenging to reliably detect even with high-resolution remotely sensed imagery, limiting our understanding of how ecosystem engineering shapes ecological processes and animal spatial behavior. In African savannas, communal dung middens created by rhinos are central to olfactory communication and nutrient redistribution, but their spatial distribution and the environmental factors shaping midden placement have not been quantified. We used coincident high-resolution thermal, RGB, and LiDAR data to detect and map rhino middens in Kruger National Park, South Africa, and demonstrate that active learning using multimodal imagery can efficiently detect middens across large areas. We then analyzed midden spatial patterning and used remotely sensed habitat metrics to quantify drivers of midden placement across spatial scales. Although we found weak and inconsistent deviations from complete spatial randomness in midden spatial patterning, midden placement was not random but strongly associated with proximity to or density of animal paths, proximity to water, and low levels of vegetation cover. These midden sites likely offer ease of access in areas of high rhino traffic that further facilitates the broadcasting of social cues. We found no relationship between midden placement and terrain attributes, suggesting that middens are placed throughout the topographic landscape, providing new insights into rhino space use. We demonstrate how using multimodal remote sensing data can facilitate a scalable approach to detecting cryptic animal-made features in heterogeneous landscapes, providing a foundation for studying broad-scale impacts of overlooked ecosystem engineering features that can be used to inform conservation strategy.

1 | Introduction

Many animals modify their environment by creating features that impact biodiversity and ecosystem function (Jones et al. 1994; Lawton 1994), promoting spatial heterogeneity. These animal-made features also provide distinct signatures of animal space use (Davies et al. 2014; Johnston and Windels 2015; van Andel et al. 2015). Mapping and quantifying animal-made features is therefore critical to advancing understanding of biogenic impacts on ecological processes and resource availability (Hastings et al. 2007; Jones et al. 1997), as well as animal spatial ecology and habitat selection, in turn enabling effective population monitoring (Crain and Bertness 2006; Johnson and Gillingham 2005; Watts

This is an open access article under the terms of the Creative Commons Attribution-NonCommercial License, which permits use, distribution and reproduction in any medium, provided the original work is properly cited and is not used for commercial purposes. All other rights reserved, including rights for text and data mining and training of artificial intelligence technologies or similar technologies.

© 2026 The Author(s). *Remote Sensing in Ecology and Conservation* published by John Wiley & Sons Ltd on behalf of Zoological Society of London.

et al. 2008). Studies of the distribution of animal-engineered landscape features are, however, limited taxonomically and often restricted to small spatial scales, in part due to challenges detecting animal-engineered features in wide-ranging species and across vast and remote areas (Andrew and Shephard 2017; Harrison et al. 2020).

Remote sensing can overcome challenges associated with mapping animal-engineered features. Multispectral satellite and airborne imagery have been used to map beaver ponds (Tape et al. 2018; Zhang et al. 2024), coral reefs (Hedley et al. 2016; Nguyen et al. 2021), and prairie dog colonies (Kearney et al. 2023), while fine-scaled features, such as ant nests, termite mounds, and grazing lawns, have been mapped with higher-resolution Light Detection and Ranging (LiDAR) and Red–Green–Blue (RGB) imagery (Davies et al. 2014; Monsimet et al. 2025; Singh et al. 2024). While advances in remote sensing technology have facilitated the mapping of an ever-expanding variety of animal-engineered features, these technologies have been most effective at mapping features with clear structural, spectral, or visible signatures. Some animal-engineered features, however, lack such clearly diagnostic characteristics and are difficult to distinguish from the surrounding environment in remotely sensed imagery (but see Andrew and Shephard 2017; Thompson et al. 2015). Our inability to reliably map these cryptic features hinders quantification of the landscape-scale distributions of many animal-made features and our broader understanding of the ecosystem engineering effects of the species creating them.

In African savannas, white (*Ceratotherium simum*) and black (*Diceros bicornis*) rhinos engineer examples of cryptic features by repeatedly defecating in communal middens used by both species for territorial marking and social communication (Figure 1; Goddard 1967; Linklater et al. 2013; Marneweck et al. 2018a; Owen-Smith 1973). Middens are found throughout rhino home ranges (Owen-Smith 1973; Goddard 1967) and likely have a strong influence on behavior and space use, but their effects cannot be fully explored without an understanding of midden spatial distribution. Moreover, middens can be substantial sites of concentrated nutrient enrichment (Veldhuis et al. 2018) that likely influence biodiversity and ecosystem function (Awasthi et al. 2024; Feeley 2005). Understanding midden distributions will therefore also provide a critical foundation for understanding rhino-engineered landscape heterogeneity, which is especially important because, as megaherbivores, rhinos are hypothesized to disproportionately impact ecosystem functioning, but their ecological role has been comparatively understudied (Hyvarinen et al. 2021; but see Cromsigt and te Beest 2014; Waldram et al. 2008). Rhinos are also severely threatened by poaching (Ferreira et al. 2015, 2018), and there is an urgent need to characterize their functional roles in areas where they still occur at relatively high densities as well as better understand their space use for conservation management.

Rhino middens, however, have never been comprehensively mapped, and thus midden spatial distribution and patterning have not been quantified. Field surveys are impractical for systematic mapping because middens are comparatively rare features spread across large rhino home ranges. Midden detection with remote sensing is also challenging due to their relatively small size (averaging 7 m in diameter, Marneweck et al. 2018a), lack of consistent three-dimensional structure, and because their color and texture can be similar to that of the surrounding landscape. Beyond rhinos, communal defecation behavior is widespread across a variety of species. Midden (or latrine) use has been shown to be important for disease transmission, mating strategies, and/or social and territorial signaling across species ranging from badgers (Böhm et al. 2008; Roper et al. 1986) and rabbits (Ziege et al. 2016) to gazelles (Wronski and Plath 2010) and lemurs (Eppley et al. 2016). Therefore, developing remote



FIGURE 1 | Rhino midden in Kruger National Park, South Africa. Photographer: Catherine A. Ressijac.

sensing tools and workflows to detect rhino middens could be applied to latrine detection across multiple species, which have, until now, exclusively relied on field-based survey methods (Carvalho et al. 2024; Kauhala and Salonen 2012; Wronski et al. 2013).

Combining multiple modalities of remote sensing imagery could circumvent midden detection challenges and provide new tools for animal-made feature mapping across a wider variety of species. While RGB and LiDAR imagery have been comparatively well used for feature mapping, they are most often used in isolation. Furthermore, other modalities, such as thermal imagery, have been less frequently used for feature mapping in ecology, despite showing promise for detecting animals (Chrétien et al. 2016; Kays et al. 2019; Seymour et al. 2017) and emissive features such as bird nests (Santangeli et al. 2020; Scholten et al. 2019). Because different remote sensing modalities measure distinct signals, combining modalities and including those less frequently used, such as thermal imagery, could provide a promising approach for detecting cryptic animal-made features.

A further challenge with using remote sensing to map animal-made features has been the ability to automate rapid and scalable feature detection (Marvin et al. 2016; Tuia et al. 2022). While machine learning models have been effective for detecting animals (Hodgson et al. 2018; Hollings et al. 2018) and a variety of animal-made features, including bird (Andrew and Shephard 2017), insect (Monsimet et al. 2025), and mammal (Kearney et al. 2023) nests and burrows, challenges persist when rare features lead to small, imbalanced datasets (Kellenberger et al. 2018) or multiple types of imagery are required for classification (Gordon et al. 2025). Integrating domain knowledge and multimodal imagery into active learning models is therefore necessary for accelerating and scaling multimodal feature mapping while maintaining detection accuracy.

Accurate and scalable detection across landscapes is key to understanding how feature distribution shapes both animal space use and the broader ecological functions that many animal-made features provide. For many such features, including latrines, placement is not random but rather influenced by environmental, social, and/or anthropogenic factors (Soultan et al. 2021; Louhichi et al. 2025). Uncovering patterns of midden site selection by rhinos can illuminate rhino space use, providing insight into habitat selection and spatial behavior as well as landscape-scale effects of middens on ecosystem function. Mapping middens and identifying drivers of midden placement thus provides a noninvasive tool for monitoring rhino space use that can advance both ecological knowledge and conservation strategy.

Here, we combine high-resolution thermal, RGB, and LiDAR imagery collected using unoccupied aerial vehicles (UAV) to map rhino middens in Kruger National Park (KNP), South Africa. We demonstrate (i) that multimodal remote sensing can be used to detect cryptic animal-made features across large landscapes and (ii) that active learning can be used for efficient detection. We then use the resulting midden maps to (iii) analyze midden spatial patterning and model the effects of key environmental variables on midden site selection (i.e., placement) by rhinos.

2 | Materials and Methods

2.1 | Study Site and Remote Sensing Data

KNP hosts the world's largest rhino population, an estimated 1850 white and 205 black rhinos in 2022 (Ferreira et al. 2024). Remote sensing data were collected over five study plots (ranging from 110 to 216 ha) in southern KNP, where rhino densities are highest, in January 2020 (mid-wet season) (Figure 2; Table 1). All plots were on granitic geology with a mean annual rainfall of 500–650 mm. The vegetation included *Acacia* thicket, Lowveld sour bushveld, and *Combretum* woodland (Gertenbach 1983), and there was a full suite of large herbivore species present.

RGB photos, thermal images, and LiDAR data were acquired simultaneously using the Harvard Animal Landscape Observatory (HALO) sensor package, which for this study consisted of a Riegl VUX-1LR LiDAR scanner, a Sony A6000 camera (24 megapixels), and a modified FLIR Tau-2 thermal camera (327,680 pixels). The sensor package was flown on a DJI M600 multicopter UAV at an altitude of 100 m above ground level at a speed of 8 m/s, parallel to the direction of the survey plots. Flight lines were spaced at 114 m to yield 60% overlap with a 110-degree field of view. The UAV's trajectory was refined using GNSS data from a StoneX S900 base station to achieve an absolute accuracy of $\leq$ 4 cm.

Thermal data were acquired every 3 s, and the imager measured thermal emission spectra between 7.5 and 13 μm at a frame rate of 30 Hz. The resulting thermal images were converted into false-color images using ThermoViewer software and an automatic color scale. All RGB and thermal images were processed in the Terrasolid software suite (Terrascan 19.030 and Terramatch 19.008) using a digital terrain model (DTM) derived from the coincident LiDAR data. The RGB and thermal images were rectified and mosaicked at a resolution of 5 cm for the RGB and 0.5 m for the thermal. LiDAR data were processed following methods outlined in Boucher et al. (2023) and Strydom et al. (2023). Briefly, point clouds created for each flight line were denoised and matching corrections applied in Terrasolid, resulting in a matching accuracy of 3–4 cm and average point density of 150 points m^{-2}. Processed LiDAR data were ground-classified and height-normalized; the relative accuracy of the LiDAR ground data was 4.5 cm.

2.2 | Midden Classification

RGB and thermal infrared orthomosaics were used to manually label midden candidates across plots. While middens have some identifiable characteristics in RGB imagery, they are difficult to distinguish from background pixels in a large, heterogeneous orthomosaic. Middens do, however, appear as bright features in thermal infrared imagery, likely due to the material properties of dung piles, such as color, density, and moisture content, that lead to increased emissivity relative to the surrounding soil and vegetation. Exothermic effects of dung decomposition (Lodha 1974)

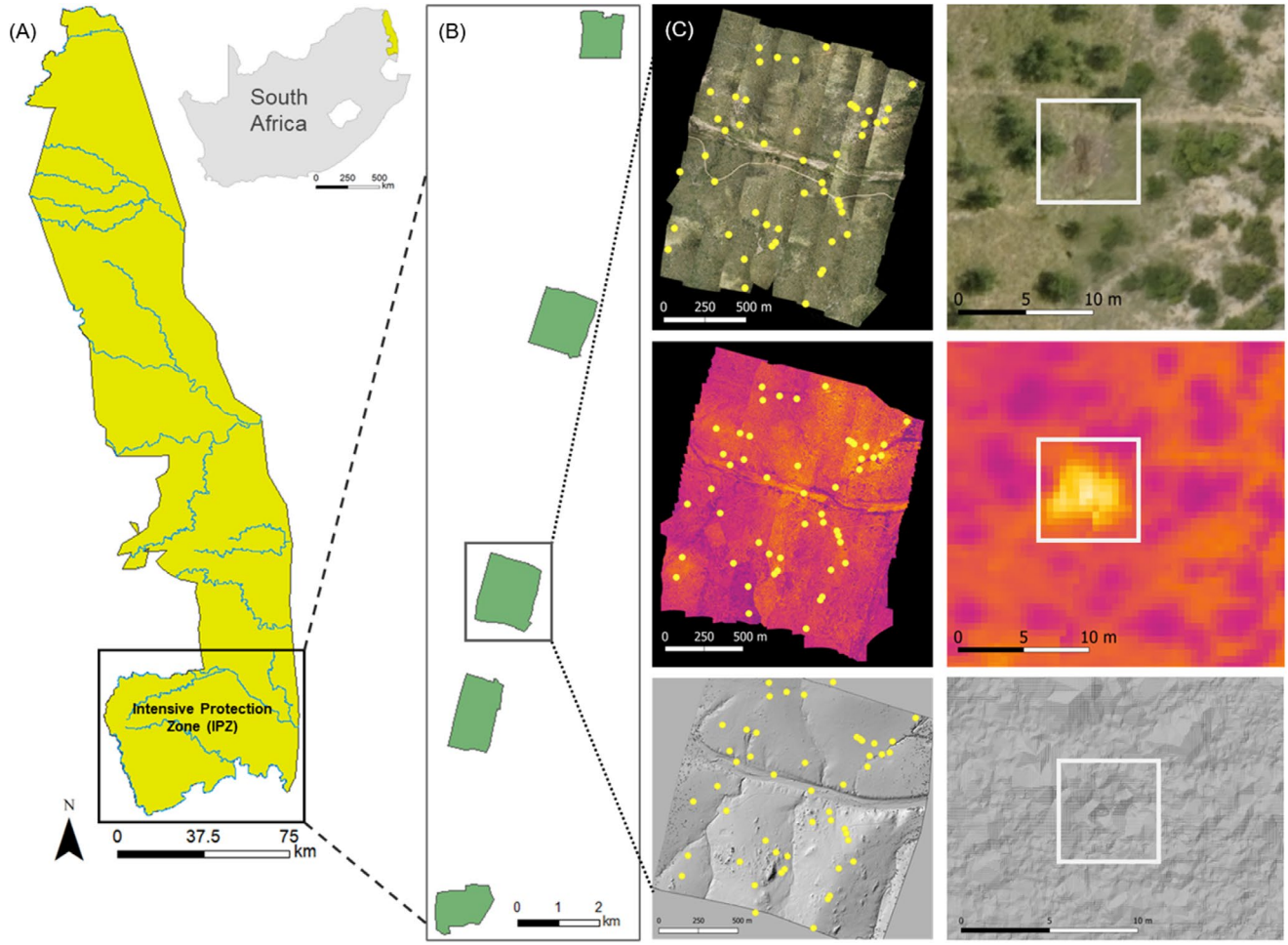


FIGURE 2 | (A) Five plots were surveyed within southern Kruger National Park, South Africa, but the exact locations are withheld for security reasons. (B) Midden locations classified in the RGB, thermal, and LiDAR imagery (top to bottom, respectively). (C) Example midden detection in the RGB (top), thermal (middle), and LiDAR (bottom) imagery.

TABLE 1 | (Left) Plot level spatial, midden, and rhino census summary statistics. (Right) Results of the nearest neighbor index (NNI) analysis of middens across the five surveyed plots, including nearest neighbor distances (NND).

	Area (ha)	Midden count	Midden density (km^{-1})	Mean annual rhino density (km^{-1})	Observed NND	Expected NND	NNI	*p*
Plot 1	110	8	7.27	3.10 ± 0.71	197.583	122.084	1.6184	0.1344
Plot 2	191	19	9.95	2.25 ± 0.21	172.614	126.991	1.359	0.0961
Plot 3	216	50	23.15	3.80 ± 0.50	100.899	86.864	1.162	0.216
Plot 4	170	10	5.88	2.65 ± 0.14	212.839	128.488	1.656	0.0561
Plot 5	118	21	17.80	0.70 ± 0.27	137.431	96.0104	1.432	0.042*

Note: NNI > 1 indicates overdispersion; however, significance tests of Monte Carlo simulations show nonsignificant deviation from complete spatial randomness in four of the five plots. * indicates $p < 0.05$.

likely also increase midden temperatures. Therefore, midden candidates were first identified in the thermal imagery and then confirmed using their shape, color, and texture characteristics visible in the RGB imagery (Figure 2B). Additionally, since male rhinos display scraping behavior at middens (Marneweck et al. 2018b; Owen-Smith 1973), hillshade models derived from the LiDAR DTMs were used to confirm middens based on shallow depressions resulting from rhino scraping (Figure 2B). However, significant scraping does not occur at all middens, so evidence of depressions was used as supportive rather than exclusive classification criteria.

A manual search for middens was conducted by a single observer across the five plots using QGIS (version 3.14.1) software. An 80

×80 m grid was constructed over each plot to guide the search and ensure all areas of each plot were covered. Candidates were only labeled as middens if conclusively identifiable in the thermal and RGB imagery. Once a midden was identified, a point was placed approximately in the center of the midden. A set of 150 candidates (both suspected midden presences and absences) was used to conduct ground presence/absence surveys across subsections of three of the five plots in September 2021 and March 2022. Using these ground data, the accuracy of the manual midden search of the remote sensing imagery was assessed by calculating performance metrics from a confusion matrix composed of true and false negative and positive counts.

Following manual detection, an active machine learning technique was applied to advance the scalability of midden mapping, adapting the MultimodAL method introduced in Gordon et al. (2023). Briefly, the MultimodAL algorithm uses multiple data modalities (e.g., thermal, RGB, and LiDAR) and employs a domain-inspired ranking technique (e.g., maximum thermal value) to overcome the problem of identifying a rare signal across an imbalanced dataset, thus increasing the probability of midden detection across data queries. We first evaluated data quality across the thermal, RGB, and LiDAR (gridded at 0.10 m resolution) imagery, excluding ~2.5% of the thermal data in plot 5 due to errors in the thermal values. Next, a 15 × 15 m grid was created over each plot in QGIS (version 3.44). Grid cells with > 50% no data pixels in all modalities (RGB, thermal, or LiDAR) were excluded, yielding 43,515 total grid cells across all plots. Grid cells containing manually detected middens were assigned a label of 1 and the rest a label of 0. Because some middens overlap multiple grid cells, 136 positive cells were obtained despite the presence of 108 manually detected middens. The minimum and maximum values in each band for each modality were computed across the valid pixels in each plot and used to rescale each grid cell to the 0–1 range. Subsequently, the grid cell was *Z*-score normalized using the pretraining statistics of the SAT-493M dataset (Siméoni et al. 2025). The DINOv3 Sat model (Siméoni et al. 2025), pretrained on the ViT-L/16 distilled architecture, was used as the frozen feature extractor for all modalities. A trainable linear layer was appended as a classifier. The single thermal and LiDAR bands were repeated three times for compatibility with the three input channels expected by DINOv3 Sat. The MultimodAL method was then run on all grid cells with a batch size of 8 cells per iteration on an NVIDIA H200 GPU with 60 GB RAM. All labeled negative cells were used, and positive cells were oversampled as needed so that negatives did not outnumber positives. Data augmentation was also used during training in the form of random horizontal and vertical flips and rotations. In each iteration, 20% of the labeled grid cells were used to form a validation set, stratified by the labels. Model selection over 10 epochs was based on the class-balanced accuracy on the validation set using a threshold of 0.5. One hundred iterations of active learning, during which 800 grid cells were labeled (< 2% of all cells), were run 10 times with different random seeds.

2.3 | Landscape Feature Processing

For analysis of midden site selection, RGB, thermal, and LiDAR imagery were used to identify landscape features hypothesized to influence midden placement by rhinos. Middens have been observed to be concentrated around drinking areas and animal trails (Owen-Smith 1973). Thus, water features were identified across the plots using a manual search of the RGB imagery, and animal paths were mapped as line features using a combination of RGB imagery and hillshade models. Only clearly defined paths identifiable at a 1:2000 m scale in QGIS were included. Additionally, since white rhinos preferentially graze at termite mounds due to the availability of nutrient-enriched vegetation (Cromsigt and te Beest 2014; Davies et al. 2016), we hypothesized that termite mounds would influence midden placement via two alternative mechanisms. First, rhino selection for areas close to or with a high density of termite mounds for improved foraging would increase the likelihood of midden placement in these high-use areas. Alternatively, since midden use has been documented as an antiparasitic strategy in many species (Hart and Hart 2018), attraction to termite mounds for grazing could result in avoidance of these areas for midden placement. Termite mounds were identified using hillshade and slope models in combination with RGB imagery to confirm mound presence (following Davies et al. 2014; Hockridge et al. 2023). Distance to water, animal paths, and termite mounds were calculated for each midden using the path distance tool in ArcMap (version 10.8.1).

Vegetation cover is known to influence habitat selection for both rhino species, with white rhinos predominantly using grassland and open wooded areas for grazing and black rhinos, as browsers, preferring areas of higher woody cover (le Roex et al. 2019; White et al. 2007). Therefore, we used the LiDAR-derived canopy height models (CHMs) to quantify vegetation cover across each plot. The highest '*z*' coordinate among first-return LiDAR points was gridded at 0.25 m spatial resolution, with outliers > 20 m excluded. A 5 × 5 m grid was overlaid on the CHMs and percent canopy cover quantified by reclassifying the CHMs into binary rasters using the R package *raster* (Hijmans and Van Etten 2012). A 1 m height threshold was used to categorize pixels as either containing woody vegetation (1) or not (0). Percent woody cover was then calculated by dividing the number of > 1 m vegetation pixels in each 5 × 5 m grid cell by the total number of pixels within the cell, generating maps of vegetation cover at 5 m resolution. Next, since rhinos tend to avoid steep or broken terrain (le Roex et al. 2020; Staegemann et al. 2026), rasters of slope and vector ruggedness measure (VRM) were generated for each plot from the LiDAR-derived DTMs (at 1 m spatial resolution) using the R package *spatialEco* (Evans and Ram 2021). Last, since the study region is dominated by undulating topography that results in ecologically relevant catenae sequences (Davies et al. 2014), relative elevation models were generated for each plot at 30 m resolution using Shuttle Radar Topography Mission (SRTM) data in SAGA GIS (version 2.3.2). The hydrology tools within SAGA GIS were used to assign a value to each pixel relative to its elevation above the nearest stream (min (stream) = 0; max (hillcrest) = 1; channel density = 5).

2.4 | Rhino Data

To quantify how rhino density might affect midden density, we used rhino sightings data from annual aerial surveys conducted by KNP management (Ferreira et al. 2015) to estimate

rhino density across the five plots. Surveys were conducted using helicopters in a block-count design described in Ferreira et al. (2015). Briefly, 3 × 3 km blocks are randomly distributed throughout southern KNP and searched annually, with the GPS location of each sighted rhino recorded. Rhino sightings data for the study area were obtained for the 2 years prior to the UAV flights (2018–2019). Since average rhino home range sizes extend beyond the area of our individual study plots, we created 20 km^2 buffers around the centroid of each plot to include surveyed rhinos whose movements, based on conservative home range estimates (le Roex et al. 2019; Pienaar et al. 1993), could include our study plots. The buffer for plot five exceeded the KNP boundary and was clipped to the extent of the reserve. Since middens used exclusively by black or white rhinos are indistinguishable in remotely sensed imagery, and because we observed the two species to share middens in our study site, we combined individual counts across species into a single rhino count. Mean annual rhino density (rhinos km^{-2}) was calculated for each buffered plot as the average of the density estimates from each survey year.

2.5 | Analysis

We conducted data analysis both among and within plots. First, midden spatial patterning was investigated at each plot using the average nearest neighbor index (NNI) and, when sample size permitted, Ripley's *K* function (plots 2, 3, and 5). Both statistics calculate interpoint distances (middens in our case) and compare observed spatial patterning to the expected distribution under complete spatial randomness. NNI provides a single point statistic representing spatial clusters (NNI < 1) or overdispersion (NNI > 1) across scales. Ripley's *K* plots a measure of point patterning against the expected measure of spatial homogeneity over a range of distances, providing insight into how clustering or dispersion changes across scales. NNI was calculated for all plots, and Monte Carlo simulations were performed to test for significant deviation from complete spatial randomness. Both NNI and Ripley's *K* were calculated using the *spatstat* package (Baddeley and Turner 2005) in R (version 4.5.2; R Core Team 2020) using a minimum convex hull to define the observation window. Correlations between rhino density and midden density were quantified using Spearman rank correlation tests for each plot.

We then constructed resource selection functions (RSF) using generalized linear mixed models (GLMMs) with a binomial distribution for analysis of midden site selection (i.e., the placement of a midden at a specific location) across the surveyed plots. Middens detected across plots were treated as the used sites ($n = 108$), and random points were generated throughout the five plots to represent available but unused sites ($n = 324$). A three to one ratio of available to used points was utilized to ensure model stability as well as thorough sampling of landscape characteristics across plots.

For each used and available point (midden or no midden), landscape metrics described above were extracted at three different spatial grain sizes, hereafter referred to as study scales: the value at the point (approximate midden center), the mean value over a circular area of ~0.2 ha (30 m radius around each point), and the mean value over a circular buffer area of ~2 ha (80 m radius around each point). A buffer radius of 30 m corresponds to the estimated distance a rhino can visually discern an object (Daniel and Mikulka 1998), and a buffer radius of 80 m corresponds to half the average nearest neighbor distance between middens across all five plots (see Results). Measurements of select landscape metrics varied between study scales to account for differences in rhino perception at varying spatial grains. At the point scale, distance to animal paths and distance to termite mounds were extracted, while at the 0.2 and 2 ha scales, animal path and termite mound density were extracted. We assessed collinearity between independent variables for each dataset across the three scales using variance inflation factors (VIF) and Pearson's correlation tests. VIF scores for all variables across the three datasets were < 2.5.

We then modeled the probability of midden site selection (1 vs. 0) as a function of percent vegetation cover, VRM, slope, relative elevation, distance to water, distance to animal paths, and distance to termite mounds at the point scale, and as a function of mean percent vegetation cover, mean VRM, mean slope, mean relative elevation, distance to water, animal path density, and termite mound density at the 0.2 and 2 ha scales (Tables 2–4). All predictor variables were scaled and centered prior to modeling. At each spatial scale, we used generalized linear mixed models (GLMMs) with a random intercept for plot to account for potential nonindependence among points within the same plot using the R package *lme4* (Bates et al. 2015). Model selection was performed by ranking models derived from each of the global models using Akaike information criteria corrected for sample size (AICc) in the R package *MuMIn* (Barton and Barton 2015). We then performed model averaging on the subset of derivative models with a delta AICc ≤ 2 relative to the best performing model (Burnham and Anderson 2002) (Tables S2–S4). Odds ratios were derived and interpreted by back-transforming model-averaged coefficients ($\exp\beta$). To assess whether the random intercept for plot adequately accounted for spatial nonindependence, we tested for residual spatial autocorrelation in each scale-specific global model using Moran's *I* on DHARMa-simulated quantile residuals, calculated separately within each of the five plots (Table S5; Hartig 2016).

We used 10-fold cross-validation to evaluate the accuracy and predictive ability of the RSFs at each spatial scale. Briefly, the set of used midden sites was randomly divided into 10 equal subsets, with 9 subsets (90% of the data) used to train the RSF model, which was then evaluated on 1 subset of testing data (the remaining 10%). This process was repeated 10 times so that each subset of data was used for testing once. The ratio of true to false positives was evaluated by plotting receiver operating characteristics (ROC) curves and computing the resulting area under the curve (AUC). Finally, we plotted individual response curves to assess relationships between each significant predictor variable and midden site selection. For each significant variable, we created a prediction dataset that included the observed range of the predictor and all other predictor variables held constant at their mean. We then calculated predicted probabilities using the model averaged datasets and generated variable effects plots, repeating the process across the three spatial scales.

3 | Results

3.1 | Midden Detection

We manually detected 108 middens across the five plots (Table 1). From our ground surveys (150 candidate sites), 49 sites were true positives, 72 were true negatives, 9 were false positives, and 20 were false negatives, with an overall detection accuracy of 81% (Table S1). Specificity was 89% and precision was 85%, revealing high confidence for both excluding midden absences and positively identifying midden presences. Sensitivity, or recall, was 71%, indicating strong detection of actual middens. Moreover, of the 20 false negatives recorded during ground surveys, 12 were middens opportunistically encountered along survey routes rather than mistakenly labeled absences. Given the 20–26-month time lapse between UAV flights and ground surveys, these 12 false negatives could represent new middens established since the flights, possibly increasing sensitivity to as high as 86%. However, activity data from middens are necessary to assess midden longevity but were unavailable for this study.

Using the manually mapped middens as reference labels, we then evaluated query efficiency and classification performance of active learning for scaling midden detection. We report results as the mean ± STD over 10 runs. After 100 rounds of active learning, during which < 2% of the total grid cells were labeled, the MultimodAL algorithm had queried 30.22% of the grid cells containing middens (Figure S1), indicating that midden-containing cells were preferentially selected at a much higher rate than expected under random sampling. Using the true labels for queried cells and model predictions for unlabeled cells, the algorithm achieved a class-balanced accuracy of 69.28% ± 0.03% across all cells (Figure S1). When evaluated on only unlabeled grid cells (that were not queried during active learning), balanced accuracy was 66.01% ± 0.02% (Figure S1), indicating that a small subset of labeled cells can be used to predict midden presence across the larger, unlabeled portion of the study area. The model achieved an ROC-AUC of 0.74 ± 0.02 on the unlabeled cells (Figure S1), demonstrating the ability to discriminate between midden and nonmidden-containing grid cells.

3.2 | Midden Spatial Patterning

The average nearest neighbor distance across the five plots was 164.273 m (SD = ±45.46). Nearest neighbor indices across all five plots indicated minor overdispersal (mean NNI = 1.445; range 1.162–1.656); however, Monte Carlo simulations showed that middens in only one plot deviated significantly ($p < 0.05$) from complete spatial randomness (Table 1). Patterns indicated by Ripley's K differed among the three plots for which these analyses were possible, with plot two showing mild but insignificant trends towards clustering at distances > 200 m, plot five showing near-significant clustering at distances > 150 m, and plot three showing significant dispersion at distances > 250 m (Figure S2).

Midden density varied at the plot level (mean = 12.81 middens/km^2; range = 5.88–23.15 middens/km^2). Across buffered plots, mean rhino density was 2.50 rhinos/km^2 (range = 0.70–3.80 rhinos/km^2) (Table 1). There was no association between mean annual rhino density and midden density ($\rho = 0.10$; $p = 0.95$).

3.3 | Midden Site Selection

All three models of midden site selection performed well, but performance varied with spatial scale, with midden site selection best predicted at the point scale (AUC = 0.87) (Figure 3). Across scales, distance to (point scale) or density of (0.2 and 2 ha scales) animal paths, vegetation cover, and distance to water were the strongest drivers of midden placement and were significant ($p < 0.05$) in all ensemble model sets (Tables 2–4; Figure 4). At each scale, middens were more likely to be located closer to

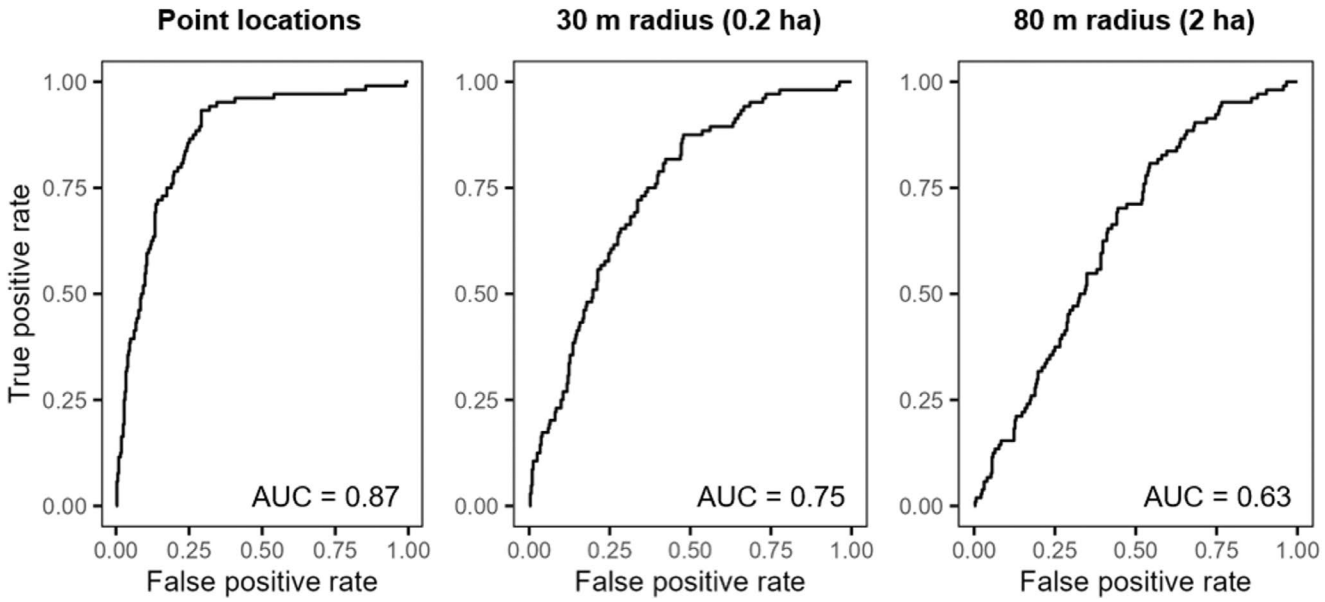


FIGURE 3 | Receiver operating characteristic (ROC) curves and area under the curve (AUC) calculations for the model ensembles used to predict midden site selection at point, 0.2 ha, and 2 ha spatial scales.

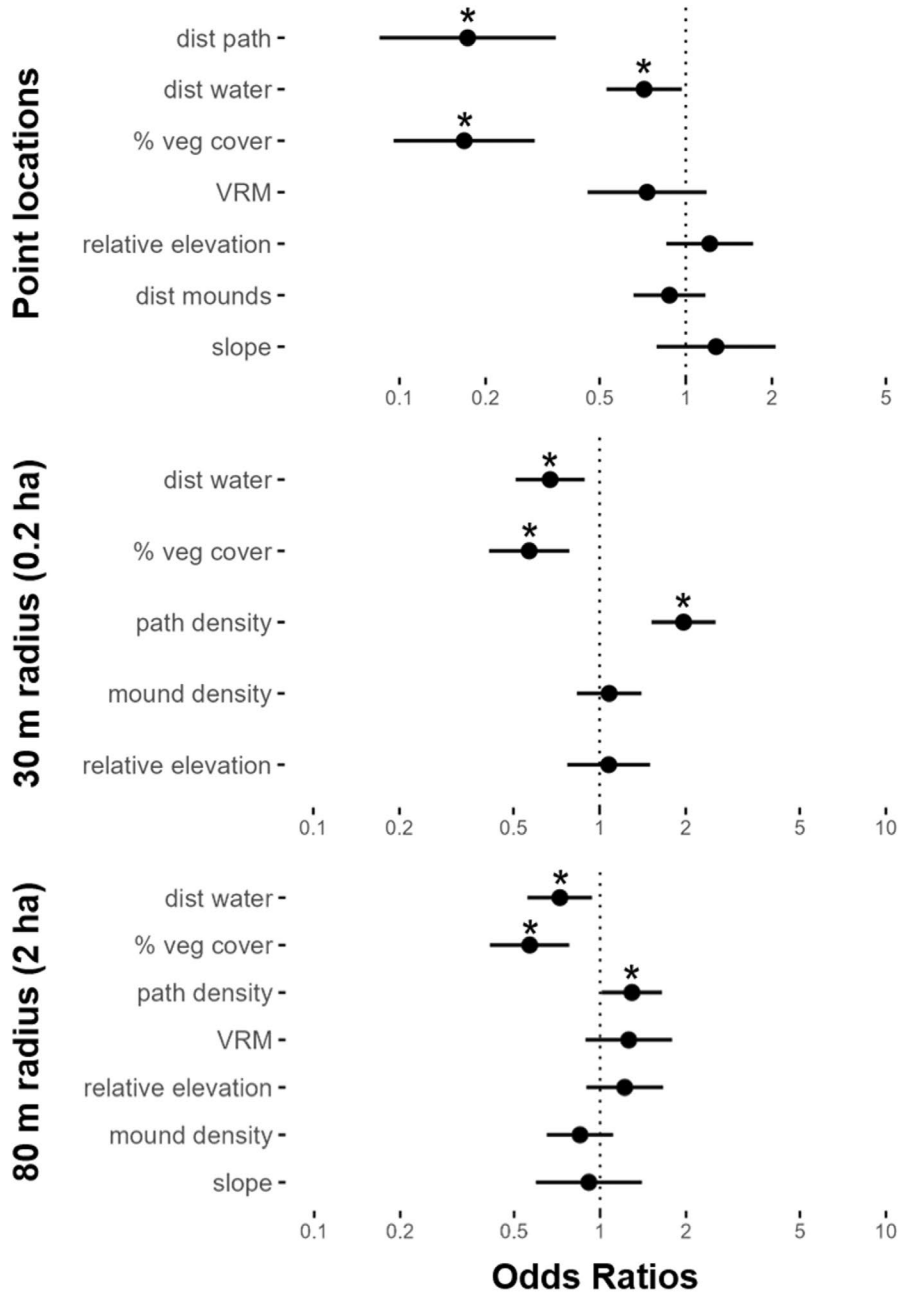


FIGURE 4 | Odds ratios (OR) with 95% confidence intervals (CI) for the predictor variables included in the model-averaged resource selection functions. * indicates $p < 0.05$. Vertical dotted line at OR = 1. Variables with OR < 1 were selected against, whereas those with OR > 1 are selected for. CI overlap of 1 indicates lack of statistical significance. Dist path = distance to animal path; dist water = distance to water; dist mound = distance to termite mound; vrm = vector ruggedness measure; %veg cover = percent vegetation cover; mean veg cover = mean vegetation cover.

or in areas with higher densities of animal paths, closer to water, and in areas of lower vegetation cover (Figures 4 and 5). At the point scale, percent vegetation cover and distance to animal paths had the largest β coefficients ($\beta > 1.7$) compared to distance to water ($\beta = -0.335$) (Table 2), while at larger scales (0.2 and 2 ha), β coefficients were more similar in magnitude across the three significant variables (Tables 3 and 4).

While the strongest predictor variables were consistent and significant across scales, the strength and shape of the relationship between each of these predictors and the probability of midden placement varied (Figure 5). At the point scale, there was strong selection for sites close to paths, with the probability of midden presence dropping to near zero 20 m from a path (Figure 5a). The relationship between path density and midden placement remained strong at the 0.2 and 2 ha scales, with positive slopes indicating midden placement was more likely at sites with a greater concentration of paths, although the slope was shallower (i.e., a weaker effect) at 2 ha (Figure 5b,c). Similarly, at the point scale there was strong selection for sites with little to no vegetation cover, with the probability of midden placement dropping to near zero when vegetation cover approached 40% (Figure 5d). This relationship remained negative but attenuated at larger scales (Figure 5e,f), with shallower and more gradual slopes at 0.2 and 2 ha. Finally, while there was a negative relationship between distance to water and midden placement at each scale, the

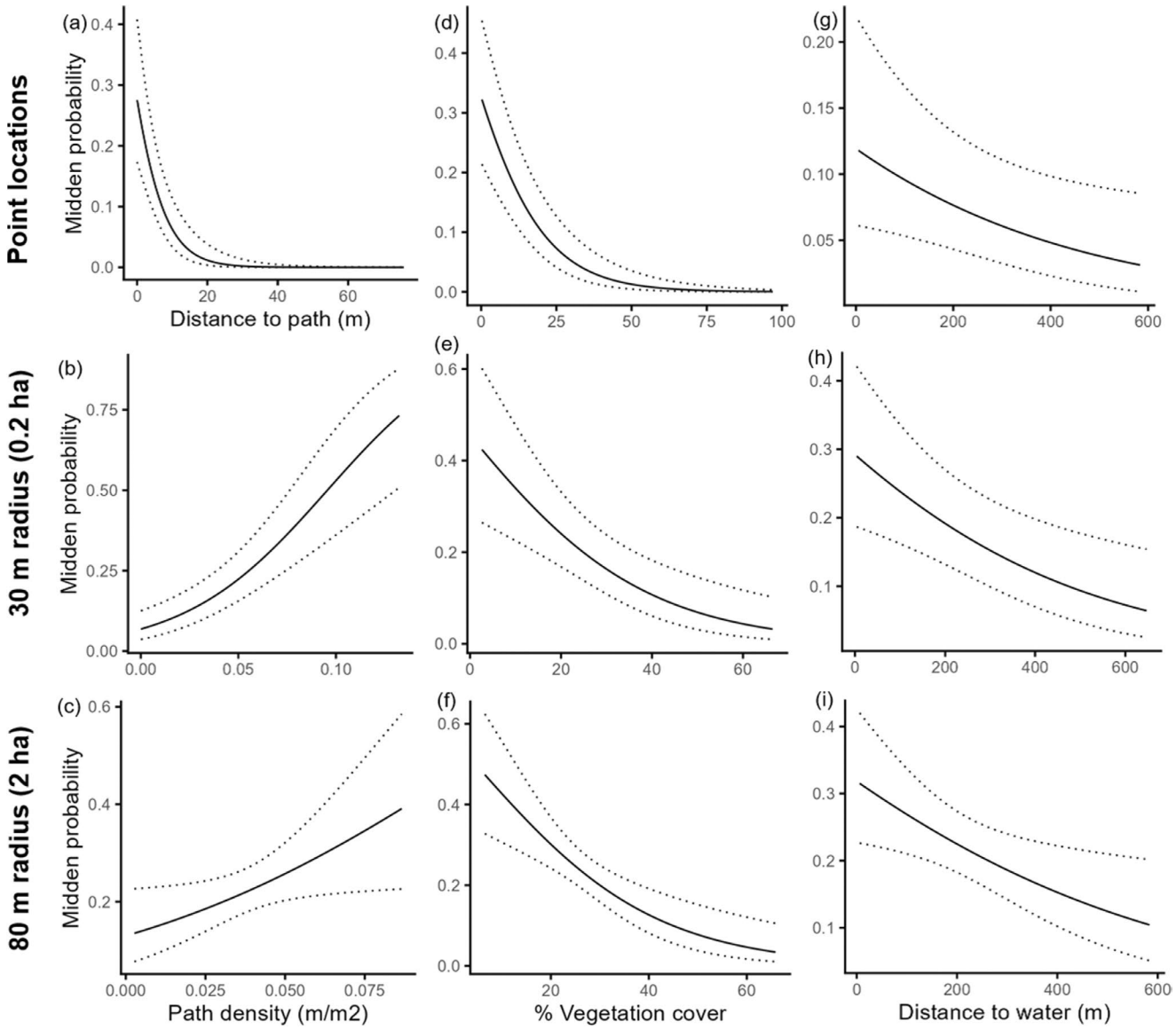


FIGURE 5 | Response curves showing the relationship between the probability of midden site selection and significant covariates, distance to path or path density (a-c), percent vegetation cover (d-f), and distance to water (g-i), across three spatial scales, derived from model-averaged predictions. Dotted lines represent 95% confidence intervals.

TABLE 2 | Model-averaged coefficients and parameter estimates from the point scale analysis of midden site selection.

Variable	β	SE (adjusted)	Z value	p	Importance
% Vegetation cover	*−1.782*	*0.289*	*6.159*	*<0.001*	*1.00*
Distance to animal paths	*−1.754*	*0.362*	*4.852*	*<0.001*	*1.00*
Distance to water	*−0.335*	*0.154*	*2.170*	*0.030*	*1.00*
Vector ruggedness measure	−0.311	0.234	0.680	0.496	0.51
Relative elevation	0.193	0.125	0.408	0.683	0.26
Distance to termite mounds	−0.131	0.088	0.326	0.744	0.22
Slope	0.244	0.112	0.243	0.808	0.11

Note: Significant variables are in italics.

TABLE 3 | Model-averaged coefficients and parameter estimates from the 0.2 ha (30 m radius) scale analysis of midden site selection.

Variable	β	SE (adjusted)	Z value	p	Importance
Animal path density	*0.675*	*0.131*	*5.142*	*<0.001*	*1.00*
% Vegetation cover	*−0.566*	*0.165*	*3.436*	*<0.001*	*1.00*
Distance to water	*−0.398*	*0.142*	*2.811*	*0.005*	*1.00*
Termite mound density	0.078	0.072	0.250	0.802	0.23
Relative elevation	0.073	0.085	0.188	0.851	0.22

Note: Significant variables are in italics.

TABLE 4 | Model-averaged coefficients and parameter estimates from the 2 ha (80 m radius) scale analysis of midden site selection.

Variable	β	SE (adjusted)	Z value	p	Importance
Distance to water	*−0.323*	*0.133*	*2.440*	*0.015*	*1.00*
% Vegetation cover	*−0.566*	*0.162*	*3.487*	*<0.001*	*1.00*
Animal path density	*0.257*	*0.124*	*2.074*	*0.038*	*1.00*
Vector ruggedness measure	0.103	0.165	0.621	0.534	0.44
Relative elevation	0.082	0.141	0.584	0.560	0.41
Termite mound density	−0.050	0.106	0.469	0.639	0.31
Slope	−0.013	0.090	0.149	0.881	0.15

Note: Significant variables are in italics.

slope was steeper (i.e., the strength of selection was stronger) at larger spatial scales (Figure 5g–i).

No terrain measure was a significant predictor of midden placement, nor was distance to or density of termite mounds (Tables 2–4).

4 | Discussion

Our study demonstrates that multimodal remote sensing can be used to detect and map cryptic animal-made features such as rhino middens in savanna landscapes. Differentiating middens from the surrounding landscape using a combination of thermal, RGB, and LiDAR data resulted in high detection accuracy (>80%), which, when paired with reduced labeling requirements through active learning, suggests that using remote sensing to map rhino middens is both reliable and scalable. We also show how concurrent multimodal data collection can be further leveraged to quantify landscape characteristics shaping site selection by animals, for example, midden placement by rhinos. Midden placement was associated with proximity to or density of animal paths, proximity to water, and reduced vegetation cover. These findings suggest that midden distributions are not random, with implications for our understanding of how middens, as both centers of social information and hypothesized nutrient hotspots, reflect rhino spatial behavior and contribute to savanna spatial heterogeneity.

The multimodal nature of our approach enabled high-performance midden mapping, with thermal data providing the highest level of midden differentiation from the surrounding vegetation. The RGB data further improved performance by providing visual shape, color, and texture details necessary for thermal candidate classification. While LiDAR alone could not be used to detect middens, these data provided a consistent signal of terrain alteration that could be used to further differentiate a suspected midden candidate. Together, the complementary strengths of each modality combined discriminative power, visual context, and 3D surface information to enable midden detection with high accuracy. Successful midden detection with remote sensing across large, heterogeneous landscapes is promising for increasing our understanding of midden placement by rhinos and other species, as well for advancing our ability to study their ecological impacts.

Our results further demonstrate the potential scalability of midden mapping by evaluating active learning performance against the manually mapped middens. MultimodAL was able to efficiently prioritize labeling effort on likely midden candidates, distinguish midden-containing from nonmidden containing cells despite a strong class imbalance in the dataset, and predict midden presence across large and heterogeneous areas with a comparatively small labeling effort. These results show that machine learning algorithms can be adapted to datasets that are highly imbalanced, have a rare signal of interest, and benefit from multiple remote sensing modalities for classification. This ability is especially relevant for mapping cryptic animal-made features such as middens at scales where comprehensive field surveys and manual imagery searches are impractical.

Our ability to map middens allowed us to analyze their spatial patterning across the study plots. Midden distributions showed minor and inconsistent deviation from complete spatial

randomness. However, our analyses and inferences were likely limited by both the size of the plots and the number of middens per plot. Similar analyses of latrine distributions in gazelles found patterns of clustering at fine spatial scales shifting toward overdispersion at larger distances (Louhichi et al. 2025). Since, like rhinos, gazelles use latrines for both social communication and territoriality (Soultan et al. 2021; Wronski and Plath 2010), we might expect to see similar patterns emerge for rhino middens with more extensive midden mapping. The relationship between rhino and midden density was also not significant, although the limited number of plots likely reduced our ability to detect density-dependent patterns. Future studies characterizing midden spatial patterning would benefit from wider, more continuous remote sensing surveys across rhino home ranges and populations.

While spatial indices showed variable and near-random midden distributions, modeling landscape drivers of midden placement clearly showed that midden placement by rhinos is structured by a distinct set of environmental variables. Using only environmental metrics, we predicted midden site selection with relatively high accuracy across three spatial scales. Animal path proximity or density, proximity to water, and low vegetation cover were the strongest predictors of midden sites across scales, consistent with field studies (Owen-Smith 1973). Strong selection for midden sites close to animal paths at the point scale likely reflects rhino movement behavior, whereas selection for areas of high path density at larger scales could be indicative of social drivers since midden placement in such high traffic areas could be strategic for maximizing olfactory broadcasting (Marneweck et al. 2018a). Selection for low vegetation cover at midden sites could be similarly strategic for scent broadcasting since open areas likely support stronger airflow that transmits olfactory compounds (Finnerty et al. 2022). Midden placement in areas of low woody cover could also indicate a preference for accessibility reflective of selection for open grazing areas by white rhino, which, across the study area, occur at much higher densities than black rhino (Ferreira et al. 2024). Preference for latrine placement in open areas has been documented in dorcas gazelles (*Gazella dorcas*) and partially attributed to enhanced predator detection (Louhichi et al. 2025); however, predation risk is much less of a concern for rhinos (Owen-Smith 1988). Finally, midden placement closer to water likely reflects broad-scale habitat selection since water is a limiting resource for African rhino species (Emslie and Adcock 2013) and has been shown to affect their movement patterns (le Roex et al. 2019; Seidel et al. 2019). However, placing middens closer to water also likely provides an opportunity for targeted social advertising at shared resources (Owen-Smith 1974; Smith et al. 2024).

We did not find a significant relationship between midden placement and any of the terrain variables considered (slope, VRM, relative elevation), suggesting that middens are placed with similar frequency across valleys, midslopes, and hillcrests. The presence of middens across undulating topography indicates that rhino space use is likely more nuanced than previous studies suggest. Previous studies found a greater likelihood of rhino occurrence in valley basins than on slopes and crests, although season and rainfall have been shown to mitigate these effects (Owen-Smith 1973; Arsenault and Owen-Smith 2011; Shrader et al. 2006; Staegemann et al. 2026). These studies used either focal observations or aerial census data, which are temporally constrained due to diurnal restrictions and infrequent sampling, and therefore, might inadequately capture variation in rhino spatial behavior. In contrast, middens are stationary points of recursive movement, and, as such, midden placement throughout the catena sequence suggests that while behaviors such as grazing or resting might occur more frequently in valley basins (Staegemann et al. 2026), shorter-duration but critical behaviors, such as midden use, occur more widely. Mapping middens, therefore, helps illuminate the full extent of rhino spatial behavior.

While our analysis provides insights into the environmental drivers of midden distributions, some site-specific limitations should be considered. First, white rhinos in KNP outnumbered black rhinos 9:1 at the time of our study (Ferreira et al. 2024). Therefore, our results primarily reflect the distribution of white rhino middens, although field observations showed that midden sharing between black and white rhino was common. Second, woody cover in our study sites was relatively low and comprised primarily of short shrubs and open woodland (Strydom et al. 2023). In more densely wooded habitats, thermal and RGB imagery could be less effective at detecting middens, especially those under tree canopies. This limitation will likely be especially relevant in black rhino dominated populations since this species selects more strongly for thickets and dense woodlands (le Roex et al. 2019), although white rhinos have also been shown to frequent woodlands in some areas and/or seasons (Owen-Smith 1988; Shrader et al. 2006). Third, our remote sensing approach does not provide information about rhino activity at middens, meaning that infrequently used or abandoned middens were likely also detected, introducing potential uncertainty into inferences about rhino space use deduced solely from midden distributions. Midden measurements and/or camera trap data could provide meaningful insights into the frequency of midden use, and therefore rhino space use, in future research. Finally, middens are centers of olfactory communication (Marneweck et al. 2017), and rhino biological and social traits, such as sex, age, territoriality and oestrous state, are also likely to influence midden placement due to differences in midden behavior between these trait groups (Marneweck et al. 2018a, 2018b). Future studies pairing midden mapping with movement or camera trap data could add to our findings and elucidate how social drivers affect midden distributions.

Despite these limitations, our results have important implications for rhino conservation and ecological impact. All rhino species are highly threatened with extinction and are intensively protected (Ferreira et al. 2015; Ferreira and Dziba 2023). Mapping middens can be a valuable, noninvasive tool for monitoring rhino space use that can inform both conservation planning and antipoaching strategy. As stationary features that are repeatedly used by multiple rhinos, middens serve as robust signals of rhino space use that persist over time. Mapping midden distributions could help identify core use areas and home range or territorial boundaries that can guide strategic planning and management interventions, complementing traditional methods used to determine rhino space use, such as aerial surveys (Ferreira et al. 2015; le Roex et al. 2020). Furthermore, midden mapping offers a novel advancement towards quantifying sources of rhino-engineered landscape heterogeneity. Rhinos redistribute

nutrients across landscapes due to their size and defecation behavior (Veldhuis et al. 2018), and nutrient enrichment at animal middens is hypothesized to influence plant community composition and soil properties (Monk et al. 2024), alter ecosystem function (Reider et al. 2024), and attract a diverse assemblage of nonrhino animal species (Awasthi et al. 2024), but they have been largely overlooked as sources of landscape heterogeneity. As rhino populations continue to decline, understanding their functional roles is critical for anticipating how rhino species loss will cascade to affect ecosystem processes. Moreover, latrine use has been documented in a wide range of species (Eisenberg and Kleiman 1972; Finnerty et al. 2022), serves a variety of ecological and social functions within these species (Buesching and Jordan 2019; Ezenwa 2004), and influences ecosystem structure and function through soil enrichment and alteration of plant diversity and community composition (Ellis-Soto et al. 2021; Monk et al. 2024; Reider et al. 2024). A more complete spatial knowledge of midden distributions across species and landscapes will aid our understanding of the extent to which these features shape both spatial ecology and environmental heterogeneity. Our findings demonstrate that high-resolution, multimodal imagery can be used to detect these cryptic animal-made features and provide insights into the environmental factors influencing their placement.

Author Contributions

Catherine A. Ressijac: conceptualization, investigation, writing – original draft, methodology, validation, visualization, formal analysis, data curation. **Lucia Gordon:** investigation, methodology, visualization, writing – review and editing, formal analysis, software. **Andrew B. Davies:** conceptualization, writing – original draft, supervision, funding acquisition, validation, investigation, project administration, data curation, resources.

Acknowledgements

Peter Boucher, Evan Hockridge, and Tom Lautenbach assisted with UAV data collection and processing. Michael Voysey and Marike Louw-Voysey assisted with ground mapping of middens. Elizabeth Bondi, Nikhil Behari, and Samuel Collier contributed to various stages of the active learning algorithm. Funding was provided by Harvard University and the US National Science Foundation (NSF) under award number DEB 2303835; L.G. was supported by an NSF Graduate Research Fellowship under award number DGE 2140743.

Funding

This work was supported by the National Science Foundation (Grants DGE 2140743 and DEB 2303835) and Harvard University.

Disclosure

Author declaration: All authors have met contribution criteria and seen and approved the submitted version of the manuscript. The manuscript has not been submitted for consideration nor published elsewhere.

Conflicts of Interest

The authors declare no conflicts of interest.

Data Availability Statement

Data underlying the study cannot be made publicly available due to the vulnerability of the study species.

References

Andrew, M. E., and J. M. Shephard. 2017. "Semi-Automated Detection of Eagle Nests: An Application of Very High-Resolution Image Data and Advanced Image Analyses to Wildlife Surveys." *Remote Sensing in Ecology and Conservation* 3, no. 2: 66–80. https://doi.org/10.1002/RSE2.38.

Arsenault, R., and N. Owen-Smith. 2011. "Competition and Coexistence Among Short-Grass Grazers in the Hluhluwe-iMfolozi Park, South Africa." 89, no. 10: 900–907. https://doi.org/10.1139/z11-067.

Awasthi, B., K. R. McConkey, S. T. Aluthwattha, C. Chen, and J. Chen. 2024. "Restoring Ecological Function: Interactions Between Vertebrates and Latrines in a Reintroduced Population of *Rhinoceros unicornis*." *Biological Conservation* 294: 110611. https://doi.org/10.1016/J.BIOCON.2024.110611.

Baddeley, A., and R. Turner. 2005. "Spatstat: An R Package for Analyzing Spatial Point Patterns." *Journal of Statistical Software* 12: 1–42. https://doi.org/10.18637/JSS.V012.I06.

Barton, K., and M. K. Barton. 2015. "Package 'Mumin'." *Version* 1, no. 18: 439.

Bates, D., M. Mächler, B. Bolker, and S. Walker. 2015. "Fitting Linear Mixed-Effects Models Using lme4." *Journal of Statistical Software* 67: 1–48. https://doi.org/10.18637/jss.v067.i01.

Böhm, M., K. L. Palphramand, G. Newton-Cross, M. R. Hutchings, and P. C. L. White. 2008. "The Spatial Distribution of Badgers, Setts and Latrines: The Risk for Intra-Specific and Badger-Livestock Disease Transmission." *Ecography* 31, no. 4: 525–537. https://doi.org/10.1111/J.0906-7590.2008.05314.X.

Boucher, P. B., E. G. Hockridge, J. Singh, and A. B. Davies. 2023. "Flying High: Sampling Savanna Vegetation With UAV-Lidar." *Methods in Ecology and Evolution* 14, no. 7: 1668–1686. https://doi.org/10.1111/2041-210X.14081.

Buesching, C. D., and N. Jordan. 2019. "The Social Function of Latrines: A Hypothesis-Driven Research Approach." In *Chemical Signals in Vertebrates 14*, 94–103. Springer. https://doi.org/10.1007/978-3-030-17616-7_8.

Burnham, K. P., and D. R. Anderson. 2002. *Model Selection and Multimodel Inference: A Practical Information-Theoretic Approach*. Springer.

Carvalho, F., B. A. Ziko, Z. Mrubata, M. Xhobani, A. Plaatjie, and E. Do Linh San. 2024. "Multi-Scale Habitat Modelling of Latrine Site Selection by Sympatric Carnivores in an Albany Thicket Landscape, South Africa." *Landscape Ecology* 39, no. 3: 43. https://doi.org/10.1007/s10980-024-01854-8.

Chrétien, L. P., J. Théau, and P. Ménard. 2016. "Visible and Thermal Infrared Remote Sensing for the Detection of White-Tailed Deer Using an Unmanned Aerial System." *Wildlife Society Bulletin* 40, no. 1: 181–191. https://doi.org/10.1002/WSB.629.

Crain, C. M., and M. D. Bertness. 2006. "Ecosystem Engineering Across Environmental Gradients: Implications for Conservation and Management." *Bioscience* 56, no. 3: 211–218. https://doi.org/10.1641/0006-3568(2006)056[0211:EEAEGI]2.0.CO;2.

Cromsigt, J. P. G. M., and M. te Beest. 2014. "Restoration of a Megaherbivore: Landscape-Level Impacts of White Rhinoceros in Kruger National Park, South Africa." *Journal of Ecology* 102, no. 3: 566–575. https://doi.org/10.1111/1365-2745.12218.

Daniel, J. C., and P. J. Mikulka. 1998. "Discrimination Learning in the White Rhinoceros." *Applied Animal Behaviour Science* 58, no. 1–2: 197–202. https://doi.org/10.1016/S0168-1591(97)00123-8.

Davies, A. B., S. R. Levick, G. P. Asner, M. P. Robertson, B. J. van Rensburg, and C. L. Parr. 2014. "Spatial Variability and Abiotic Determinants of Termite Mounds Throughout a Savanna Catchment." *Ecography* 37, no. 9: 852–862. https://doi.org/10.1111/ecog.00532.

Davies, A. B., S. R. Levick, M. P. Robertson, B. J. van Rensburg, G. P. Asner, and C. L. Parr. 2016. "Termite Mounds Differ in Their Importance for Herbivores Across Savanna Types, Seasons and Spatial Scales." *Oikos* 125, no. 5: 726–734. https://doi.org/10.1111/OIK.02742.

Eisenberg, J. F., and D. G. Kleiman. 1972. "Olfactory Communication in Mammals." *Annual Review of Ecology and Systematics* 3: 1–32. https://doi.org/10.1146/annurev.es.03.110172.000245.

Ellis-Soto, D., K. M. Ferraro, M. Rizzuto, E. Briggs, J. D. Monk, and O. J. Schmitz. 2021. "A Methodological Roadmap to Quantify Animal-Vectored Spatial Ecosystem Subsidies." *Journal of Animal Ecology* 90, no. 7: 1605–1622. https://doi.org/10.1111/1365-2656.13538.

Emslie, R. H., and K. Adcock. 2013. "*Diceros bicornis* Black Rhinoceros." In *The Mammals of Africa*, vol. 5, 455–544. Bloomsbury Publishing.

Eppley, T. M., J. U. Ganzhorn, and G. Donati. 2016. "Latrine Behaviour as a Multimodal Communicatory Signal Station in Wild Lemurs: The Case of *Hapalemur meridionalis*." *Animal Behaviour* 111: 57–67. https://doi.org/10.1016/J.ANBEHAV.2015.10.012.

Evans, J. S., and K. Ram. 2021. "Package 'spatialEco.' R CRAN Project."

Ezenwa, V. O. 2004. "Selective Defecation and Selective Foraging: Antiparasite Behavior in Wild Ungulates?" *Ethology* 110, no. 11: 851–862. https://doi.org/10.1111/j.1439-0310.2004.01013.x.

Feeley, K. 2005. "The Role of Clumped Defecation in the Spatial Distribution of Soil Nutrients and the Availability of Nutrients for Plant Uptake." *Journal of Tropical Ecology* 21, no. 1: 99–102. https://doi.org/10.1017/S0266467404001701.

Ferreira, S. M., E. T. Crowhurst, C. Greaver, and C. Simms. 2024. "Resizing Kruger National Park: Trends in Numbers of Rhinoceroses Within Priority Zones." *Koedoe* 66, no. 1: 1802.

Ferreira, S. M., and L. Dziba. 2023. "Rhinoceros Accounting in Kruger National Park, South Africa." *Journal for Nature Conservation* 72: 126359. https://doi.org/10.1016/j.jnc.2023.126359.

Ferreira, S. M., C. Greaver, G. A. Knight, M. H. Knight, I. P. J. Smit, and D. Pienaar. 2015. "Disruption of Rhino Demography by Poachers May Lead to Population Declines in Kruger National Park, South Africa." *PLoS One* 10, no. 6: e0127783. https://doi.org/10.1371/journal.pone.0127783.

Ferreira, S. M., C. Greaver, Z. Nhleko, and C. Simms. 2018. "Realization of Poaching Effects on Rhinoceroses in Kruger National Park, South Africa." *African Journal of Wildlife Research* 48, no. 1: 013001. https://doi.org/10.3957/056.048.013001.

Finnerty, P. B., C. Mcarthur, P. Banks, C. Price, and A. M. Shrader. 2022. "The Olfactory Landscape Concept: A Key Source of Past, Present, and Future Information Driving Animal Movement and Decision-Making." *Bioscience* 72, no. 8: 745–752. https://doi.org/10.1093/BIOSCI/BIAC039.

Gertenbach, W. P. D. 1983. "Landscapes of the Kruger National Park." *Koedoe* 26, no. 1: 9–121. https://doi.org/10.4102/KOEDOE.V26I1.591.

Goddard, J. 1967. "Home Range, Behaviour, and Recruitment Rates of Two Black Rhinoceros Populations." *African Journal of Ecology* 5, no. 1: 133–150. https://doi.org/10.1111/J.1365-2028.1967.TB00768.X.

Gordon, L., N. Behari, S. Collier, et al. 2023. "Find Rhinos Without Finding Rhinos: Active Learning With Multimodal Imagery of South African Rhino Habitats." In *Proceedings of the Thirty-Second International Joint Conference on Artificial Intelligence {IJCAI-23}*, edited by E. Elkind, 5977–5985. International Joint Conferences on Artificial Intelligence Organization. https://doi.org/10.24963/ijcai.2023/663.

Gordon, L., N. Lang, C. Ressijac, and A. Davies. 2025. "Multimodal Fusion Strategies for Mapping Biophysical Landscape Features." In *Computer Vision—ECCV 2024 Workshops*, edited by A. Del Bue, C. Canton, J. Pont-Tuset, and T. Tommasi, 208–216. Springer Nature Switzerland.

Harrison, L. R., C. J. Legleiter, B. T. Overstreet, T. W. Bell, and J. Hannon. 2020. "Assessing the Potential for Spectrally Based Remote Sensing of Salmon Spawning Locations." *River Research and Applications* 36, no. 8: 1618–1632. https://doi.org/10.1002/RRA.3690.

Hart, B. L., and L. A. Hart. 2018. "How Mammals Stay Healthy in Nature: The Evolution of Behaviours to Avoid Parasites and Pathogens." *Philosophical Transactions of the Royal Society, B: Biological Sciences* 373, no. 1751: 20170205. https://doi.org/10.1098/RSTB.2017.0205.

Hartig, F. 2016. *DHARMa: Residual Diagnostics for Hierarchical (Multi-Level/Mixed) Regression Models*. CRAN: Contributed Packages.

Hastings, A., J. E. Byers, J. A. Crooks, et al. 2007. "Ecosystem Engineering in Space and Time." *Ecology Letters* 10, no. 2: 153–164. https://doi.org/10.1111/J.1461-0248.2006.00997.X.

Hedley, J. D., C. M. Roelfsema, I. Chollett, et al. 2016. "Remote Sensing of Coral Reefs for Monitoring and Management: A Review." *Remote Sensing* 8, no. 2: 118. https://doi.org/10.3390/RS8020118.

Hijmans, R. J., and J. Van Etten. 2012. "raster: Geographic Analysis and Modeling With Raster Data." R package version 2.0-12.

Hockridge, E. G., J. Singh, P. B. Boucher, and A. B. Davies. 2023. "Resistance of Termite Mounds to Variation in Long-Term Fire Regimes Across Semi-Arid African Savannas." *Journal of Animal Ecology* 92, no. 7: 1294–1305. https://doi.org/10.1111/1365-2656.13830.

Hodgson, J. C., R. Mott, S. M. Baylis, et al. 2018. "Drones Count Wildlife More Accurately and Precisely Than Humans." *Methods in Ecology and Evolution* 9, no. 5: 1160–1167. https://doi.org/10.1111/2041-210X.12974.

Hollings, T., M. Burgman, M. van Andel, M. Gilbert, T. Robinson, and A. Robinson. 2018. "How Do You Find the Green Sheep? A Critical Review of the Use of Remotely Sensed Imagery to Detect and Count Animals." *Methods in Ecology and Evolution* 9, no. 4: 881–892. https://doi.org/10.1111/2041-210X.12973.

Hyvarinen, O., M. Te Beest, E. le Roux, et al. 2021. "Megaherbivore Impacts on Ecosystem and Earth System Functioning: The Current State of the Science." *Ecography* 44, no. 11: 1579–1594. https://doi.org/10.1111/ECOG.05703.

Johnson, C. J., and M. P. Gillingham. 2005. "An Evaluation of Mapped Species Distribution Models Used for Conservation Planning." *Environmental Conservation* 32, no. 2: 117–128. https://doi.org/10.1017/S0376892905002171.

Johnston, C. A., and S. K. Windels. 2015. "Using Beaver Works to Estimate Colony Activity in Boreal Landscapes." *Journal of Wildlife Management* 79, no. 7: 1072–1080. https://doi.org/10.1002/JWMG.927.

Jones, C. G., J. H. Lawton, and M. Shachak. 1994. "Organisms as Ecosystem Engineers." *Oikos* 69: 373–386. https://doi.org/10.2307/3545850.

Jones, C. G., J. H. Lawton, and M. Shachak. 1997. "Positive and Negative Effects of Organisms as Physical Ecosystem Engineers." *Ecology* 78, no. 7: 1946. https://doi.org/10.2307/2265935.

Kauhala, K., and L. Salonen. 2012. "Does a Non-Invasive Method—Latrine Surveys—Reveal Habitat Preferences of Raccoon Dogs and Badgers?" *Mammalian Biology* 77, no. 4: 264–270. https://doi.org/10.1016/J.MAMBIO.2012.02.007.

Kays, R., J. Sheppard, K. Mclean, et al. 2019. "Hot Monkey, Cold Reality: Surveying Rainforest Canopy Mammals Using Drone-Mounted Thermal Infrared Sensors." *International Journal of Remote Sensing* 40, no. 2: 407–419. https://doi.org/10.1080/01431161.2018.1523580.

Kearney, S. P., L. M. Porensky, D. J. Augustine, and D. W. Pellatz. 2023. "Toward Broad-Scale Mapping and Characterization of Prairie Dog Colonies From Airborne Imagery Using Deep Learning." *Ecological Indicators* 154: 110684. https://doi.org/10.1016/J.ECOLIND.2023.110684.

Kellenberger, B., D. Marcos, and D. Tuia. 2018. "Detecting Mammals in UAV Images: Best Practices to Address a Substantially Imbalanced Dataset With Deep Learning." *Remote Sensing of Environment* 216: 139–153. https://doi.org/10.1016/j.rse.2018.06.028.

Lawton, J. H. 1994. "What Do Species Do in Ecosystems?" *Oikos* 71: 367–374. https://doi.org/10.2307/3545824.

le Roex, N., C. Dreyer, and S. M. Ferreira. 2020. "Poaching Creates Ecological Traps Within an Iconic Protected Area." *Animal Conservation* 23, no. 3: 250–259. https://doi.org/10.1111/ACV.12532.

le Roex, N., C. Dreyer, P. Viljoen, M. Hofmeyr, and S. M. Ferreira. 2019. "Seasonal Space-Use and Resource Limitation in Free-Ranging Black Rhino." *Mammalian Biology* 99, no. 1: 81–87. https://doi.org/10.1016/J.MAMBIO.2019.11.001.

Linklater, W. L., K. Mayer, and R. R. Swaisgood. 2013. "Chemical Signals of Age, Sex and Identity in Black Rhinoceros." *Animal Behaviour* 85, no. 3: 671–677. https://doi.org/10.1016/J.ANBEHAV.2012.12.034.

Lodha, B. C. 1974. "Decomposition of Digested Litter." *Biology of Plant Litter Decomposition* 1: 213–241. https://doi.org/10.1016/B978-0-12-215001-2.50013-1.

Louhichi, M., M. Petretto, O. T. Hmidi, et al. 2025. "Environmental and Spatial Drivers of Latrine Site Selection in Dorcas Gazelle." *Ecology and Evolution* 15, no. 8: e71800. https://doi.org/10.1002/ECE3.71800.

Marneweck, C., A. Jürgens, and A. M. Shrader. 2017. "Dung Odours Signal Sex, Age, Territorial and Oestrous State in White Rhinos." *Proceedings of the Royal Society B: Biological Sciences* 284, no. 1846: 20162376. https://doi.org/10.1098/rspb.2016.2376.

Marneweck, C., A. Jürgens, and A. M. Shrader. 2018a. "The Role of Middens in White Rhino Olfactory Communication." *Animal Behaviour* 140: 7–18. https://doi.org/10.1016/j.anbehav.2018.04.001.

Marneweck, C., A. Jürgens, and A. M. Shrader. 2018b. "Ritualised Dung Kicking by White Rhino Males Amplifies Olfactory Signals but Reduces Odour Duration." *Journal of Chemical Ecology* 44, no. 10: 875–885. https://doi.org/10.1007/S10886-018-0988-3.

Marvin, D. C., L. P. Koh, A. J. Lynam, et al. 2016. "Integrating Technologies for Scalable Ecology and Conservation." *Global Ecology and Conservation* 7: 262–275. https://doi.org/10.1016/J.GECCO.2016.07.002.

Monk, J. D., E. Donadio, P. F. Gregorio, and O. J. Schmitz. 2024. "Vicuña Antipredator Diel Movement Drives Spatial Nutrient Subsidies in a High Andean Ecosystem." *Ecology* 105, no. 3: e4262. https://doi.org/10.1002/ECY.4262.

Monsimet, J., S. Sjögersten, N. J. Sanders, M. Jonsson, J. Olofsson, and M. Siewert. 2025. "UAV Data and Deep Learning: Efficient Tools to Map Ant Mounds and Their Ecological Impact." *Remote Sensing in Ecology and Conservation* 11, no. 1: 5–19. https://doi.org/10.1002/RSE2.400.

Nguyen, T., B. Liquet, K. Mengersen, and D. Sous. 2021. "Mapping of Coral Reefs With Multispectral Satellites: A Review of Recent Papers." *Remote Sensing* 13, no. 21: 4470. https://doi.org/10.3390/RS13214470.

Owen-Smith, N. 1973. *The Behavioural Ecology of the White Rhinoceros*. University of Wisconsin.

Owen-Smith, R. N. 1974. "The Social System of the White Rhinoceros." *Conference on the Behaviour of Ungulates and Its Relation to Management*.

Owen-Smith, R. N. 1988. *Megaherbivores: The Influence of Very Large Body Size on Ecology*. Cambridge University Press.

Pienaar, D. J., J. D. P. Bothma, and G. K. Theron. 1993. "Landscape Preference of the White Rhinoceros in the Central and Northern Kruger National Park." *Koedoe* 36, no. 1: 79–85. https://doi.org/10.4102/KOEDOE.V36I1.364.

R Core Team. 2020. *R: A Language and Environment for Statistical Computing*. R Foundation for Statistical Computing.

Reider, K. E., C. P. Bueno de Mesquita, K. Anderson, et al. 2024. "Wild Andean Camelids Promote Rapid Ecosystem Development After Glacier Retreat." *Scientific Reports* 14, no. 1: 31913. https://doi.org/10.1038/S41598-024-83457-6.

Roper, T. J., D. J. Shepherdson, and J. M. Davies. 1986. "Scent Marking With Faeces and Anal Secretion in the European Badger (*Meles meles*): Seasonal and Spatial Characteristics of Latrine Use in Relation to Territoriality." *Behaviour* 97, no. 1–2: 94–117. https://doi.org/10.1163/156853986X00333.

Santangeli, A., Y. Chen, E. Kluen, R. Chirumamilla, J. Tiainen, and J. Loehr. 2020. "Integrating Drone-Borne Thermal Imaging With Artificial Intelligence to Locate Bird Nests on Agricultural Land." *Scientific Reports* 10, no. 1: 10993. https://doi.org/10.1038/s41598-020-67898-3.

Scholten, C. N., A. J. Kamphuis, K. J. Vredevoogd, et al. 2019. "Real-Time Thermal Imagery From an Unmanned Aerial Vehicle Can Locate Ground Nests of a Grassland Songbird at Rates Similar to Traditional Methods." *Biological Conservation* 233: 241–246. https://doi.org/10.1016/J.BIOCON.2019.03.001.

Seidel, D. P., W. L. Linklater, W. Kilian, P. Du Preez, and W. M. Getz. 2019. "Mesoscale Movement and Recursion Behaviors of Namibian Black Rhinos." *Movement Ecology* 7, no. 1: 1–14. https://doi.org/10.1186/S40462-019-0176-2.

Seymour, A. C., J. Dale, M. Hammill, P. N. Halpin, and D. W. Johnston. 2017. "Automated Detection and Enumeration of Marine Wildlife Using Unmanned Aircraft Systems (UAS) and Thermal Imagery." *Scientific Reports* 7, no. 1: 45127. https://doi.org/10.1038/srep45127.

Shrader, A. M., N. Owen-Smith, and J. O. Ogutu. 2006. "How a Mega-Grazer Copes With the Dry Season: Food and Nutrient Intake Rates by White Rhinoceros in the Wild." *Functional Ecology* 20, no. 2: 376–384. https://doi.org/10.1111/j.1365-2435.2006.01107.x.

Siméoni, O., H. V. Vo, M. Seitzer, et al. 2025. "Dinov3." *ArXiv Preprint*. ArXiv:2508.10104.

Singh, J., J. E. Donaldson, S. Archibald, C. L. Parr, M. D. Voysey, and A. B. Davies. 2024. "Small-Scale Fires Interact With Herbivore Feedbacks to Create Persistent Grazing Lawn Environments." *Journal of Applied Ecology* 61: 1531–1545. https://doi.org/10.1111/1365-2664.14645.

Smith, E., L. R. Brown, and A. S. Barrett. 2024. "Insights Into Artificial Waterhole Utilization Patterns by Elephants and Rhinos: Lessons From a South African Nature Reserve." *PLoS One* 19, no. 10: e0312158. https://doi.org/10.1371/journal.pone.0312158.

Soultan, A., A. Nagy, and O. Attum. 2021. "Midden Site Selection in Dorcas Gazelle: Larger Is Not Always Better." *Ecology and Evolution* 11, no. 20: 13661–13667. https://doi.org/10.1002/ECE3.8141.

Staegemann, E. S. M., T. Kuiper, D. J. Druce, G. I. H. Kerley, S. Mbongwa, and J. P. G. M. Cromsigt. 2026. "Resource Availability and Human Activity Shape the Landscape Distribution of White Rhinoceros, a Highly Threatened African Megaherbivore." *Oecologia* 208, no. 2: 31. https://doi.org/10.1007/S00442-025-05845-7.

Strydom, T., I. P. J. Smit, N. Govender, et al. 2023. "High-Intensity Fires May Have Limited Medium-Term Effectiveness for Reversing Woody Plant Encroachment in an African Savanna." *Journal of Applied Ecology* 60, no. 4: 661–672. https://doi.org/10.1111/1365-2664.14362.

Tape, K. D., B. M. Jones, C. D. Arp, I. Nitze, and G. Grosse. 2018. "Tundra Be Dammed: Beaver Colonization of the Arctic." *Global Change Biology* 24, no. 10: 4478–4488. https://doi.org/10.1111/GCB.14332.

Thompson, S., G. Thompson, J. Sackmann, J. Spark, and T. Brown. 2015. "Using High-Definition Aerial Photography to Search in 3D for Malleefowl Mounds Is a Cost-Effective Alternative to Ground Searches." *Pacific Conservation Biology* 21, no. 3: 208–213. https://doi.org/10.1071/PC14919.

Tuia, D., B. Kellenberger, S. Beery, et al. 2022. "Perspectives in Machine Learning for Wildlife Conservation." *Nature Communications* 13: 792. https://doi.org/10.1038/s41467-022-27980-y.

van Andel, A. C., S. A. Wich, C. Boesch, et al. 2015. "Locating Chimpanzee Nests and Identifying Fruiting Trees With an Unmanned Aerial Vehicle." *American Journal of Primatology* 77, no. 10: 1122–1134. https://doi.org/10.1002/AJP.22446.

Veldhuis, M. P., M. I. Gommers, H. Olff, and M. P. Berg. 2018. "Spatial Redistribution of Nutrients by Large Herbivores and Dung Beetles in a Savanna Ecosystem." *Journal of Ecology* 106, no. 1: 422–433. https://doi.org/10.1111/1365-2745.12874.

Waldram, M. S., W. J. Bond, and W. D. Stock. 2008. "Ecological Engineering by a Mega-Grazer: White Rhino Impacts on a South African Savanna." *Ecosystems* 11, no. 1: 101–112. https://doi.org/10.1007/S10021-007-9109-9.

Watts, B. D., G. D. Therres, and M. A. Byrd. 2008. "Recovery of the Chesapeake Bay Bald Eagle Nesting Population." *Journal of Wildlife Management* 72, no. 1: 152–158. https://doi.org/10.2193/2005-616.

White, A. M., R. R. Swaisgood, and N. Czekala. 2007. "Ranging Patterns in White Rhinoceros, *Ceratotherium simum simum*: Implications for Mating Strategies." *Animal Behaviour* 74, no. 2: 349–356. https://doi.org/10.1016/J.ANBEHAV.2006.12.011.

Wronski, T., and M. Plath. 2010. "Characterization of the Spatial Distribution of Latrines in Reintroduced Mountain Gazelles: Do Latrines Demarcate Female Group Home Ranges?" *Journal of Zoology* 280, no. 1: 92–101. https://doi.org/10.1111/j.1469-7998.2009.00643.x.

Wronski, T., M. Zafar-ul Islam, and M. Plath. 2013. "Latrine Survey as a Method to Estimate the Population Size of Arabian Gazelles (*Gazella arabica*)." *Mammalian Biology* 78, no. 3: 226–230. https://doi.org/10.1016/J.MAMBIO.2012.07.158.

Zhang, W., B. Hu, G. Brown, and S. Meyer. 2024. "Beaver Pond Identification From Multi-Temporal and Multi-Sourced Remote Sensing Data." *Geo-Spatial Information Science* 27, no. 4: 953–967. https://doi.org/10.1080/10095020.2023.2183144.

Ziege, M., D. Bierbach, S. Bischoff, et al. 2016. "Importance of Latrine Communication in European Rabbits Shifts Along a Rural-To-Urban Gradient." *BMC Ecology* 16: 29. https://doi.org/10.1186/s12898-016-0083-y.

Supporting Information

Additional supporting information can be found online in the Supporting Information section. **Table S1:** Confusion matrix summarizing manual midden detection in the remote sensing imagery (September 2020) versus detection of middens from KNP ground truth surveys (September 2021 and March 2022). **Table S2:** Component logistic regression models with a delta AICc ≤2 relative to the best performing model, used to perform model averaging at the point location scale. Degrees of freedom (df) includes fixed effects and the plot-level random intercept. *indicates $p < 0.05$. Veg_cover = vegetation cover (%); dist_path = distance to animal path; dist_water = distance to water; dist_mound = distance to termite mound; rel_elev = relative elevation; vrm = vector ruggedness measure. **Table S3:** Component logistic regression models with a delta AICc ≤2 relative to the best performing model, used to perform model averaging at the 0.2 ha (30 m radius) scale. Degrees of freedom (df) includes fixed effects and the plot-level random intercept. *indicates $p < 0.05$. Veg_cover = vegetation cover (%); dist_water = distance to water; path_dens = path density; rel_elev = relative elevation; mound_dens = termite mound density. **Table S4:** Component logistic regression models with a delta AICc ≤2 relative to the best performing model, used to perform model averaging at the 2 ha (80 m radius) scale. Degrees of freedom (df) includes fixed effects and the plot-level random intercept. *indicates $p < 0.05$. Veg_cover = vegetation cover (%); dist_water = distance to water; mound_dens = termite mound density; path_dens = animal path density; rel_elev = relative elevation; vrm = vector ruggedness measure. **Table S5:** Results from the Moran's *I* tests for residual spatial autocorrelation in the GLMMs at each spatial scale, calculated within each of the five study plots. Nonsignificant *p* values ($p > 0.05$) indicate no evidence of residual spatial autocorrelation after accounting for the plot-level random effect. **Figure S1:** Active learning performance over 100 iterations. Ten individual runs (blue lines) were conducted. Red lines indicate mean values computed across runs, reported as mean ± SD after 100 iterations. (A) Fraction of midden containing grid cells queried (0.302). (B) ROC-AUC of the active learning model on unlabeled cells (0.74 ± 0.02). (C) Overall class-balanced accuracy of the active learning algorithm calculated using true labels for queried cells and model predictions for unlabeled cells (69.28% ± 0.03%). (D) Balanced accuracy evaluated on unlabeled grid cells that were not queried during active learning (66.01% ± 0.02%). **Figure S2:** Results of Ripley's *K* analysis of middens across three of the surveyed plots with sufficient midden sample size. The red dashed line depicts midden distribution under complete spatial randomness, whereas the solid line shows observed midden distribution across distance in m (*x*-axis). Values above the red dashed line indicate clustering, whereas those below indicate overdispersion. The gray envelope represents 95% confidence intervals, with values outside the envelope indicating significant deviation from complete spatial randomness.